Role of friction-induced torque in stick-slip motion

Julien Scheibert, Dag Kristian Dysthe

Role of friction-induced torque in stick-slip motion

J. Scheibert[1,*] and D.K. Dysthe[1]

[1] *PGP, University of Oslo, P.O. Box 1048 Blindern, 0316 Oslo, Norway*

We present a minimal quasistatic 1D model describing the kinematics of the transition from static friction to stick-slip motion of a linear elastic block on a rigid plane. We show that, in the most generic conditions, the kinematics of both the precursors to frictional sliding and the periodic stick-slip motion are controlled by the amount of friction-induced torque at the interface. Our results allow to explain a series of recent experimental observations, in particular the nucleation location of micro-slip instabilities and the build up of an asymmetric interfacial pressure field.

Interfacial friction [1–4] plays a major role in seismology [5], biology [2, 6] and nanomechanics [4]. The frictional behavior of a contact interface is controlled by the shear strength field $\sigma_c(\mathbf{x})$, where $\mathbf{x}$ is the position in the interface. When an increasing shear force is applied, a slip region nucleates at the first point where the shear stress reaches the shear strength and grows through the propagation of a micro-slip front. Macroscopic sliding only starts after the entire interface has slipped. This general picture has provided the basis for friction models for decades [7–9]. Recently, transitions from static to kinetic friction have received renewed interest due to experiments that allow the local dynamics of frictional interfaces to be directly measured (see e.g. [10–12]). Depending on the contact configuration, very different kinds of transitions are observed.

For contacts between bodies having different shapes (for instance a sphere on a plane) the transition is smooth. As the shear force is increased, micro-slip occurs immediately at the periphery of the contact where the pressure vanishes, and the slip zone quasistatically invades the higher pressure central region [12]. For multicontacts (contacts between rough solids), this behavior was predicted decades ago using Amontons' law of friction ($\sigma_c(\mathbf{x})=\mu_s p(\mathbf{x})$ where p is the pressure and μ is the friction coefficient) [13].

For planar contacts, in which $\sigma_c(\mathbf{x})$ is expected to be essentially homogeneous, the nucleation region should occur at random locations due to unavoidable heterogeneities. Surprisingly, in most experiments, micro-slip starts at the trailing edge of the contact and propagates dynamically towards the leading edge [11, 14–17]. This behavior has not yet been clearly interpreted. Recent experiments on multicontacts interfaces also show that the onset of sliding is preceded by a series of precursors of increasing length, which arrest before reaching the interface's leading edge [15, 17]. These precursors have also been observed indirectly in microstructured contacts [16]. The dynamics reported in [11, 15, 17] have recently been reproduced in a 1D spring-block model in which the interface obeys a complex dynamics described by arrays of springs having a distribution of detachment force thresholds and a constant delay time for reattachement [9]. However, no general understanding of how the locations, directions and sizes of these precursors are selected has emerged. Moreover, the growth of an asymmetric pressure field, with a minimum near the trailing edge, which is retained during macroscopic motion [15, 17] is still unexplained.

In this Letter, we present a minimal 1D quasistatic model for a sheared planar frictional interface. By accounting explicitly for the friction-induced torque that arises in virtually all practical situations, we reproduce the above-mentioned unexplained observations. This provides a comprehensive picture of the kinematics of the transition from static friction to periodic stick-slip motion, including precursors.

Model - We consider the setup sketched in Fig. 1. A frictional interface is formed by pressing a linear elastic block (Young's modulus E, thickness t, width w and length L, perfectly bonded to a rigid plate) on a horizontal plane. The normal load N is applied symmetrically with respect to the contact center. The tangential displacement of the plate, X, is prescribed at a height H with respect to the frictional interface, giving rise to a friction force F. We assume small deformations, *i.e.* $N, F < 10^{-3}EwL$. We assume Amontons' rigid-plastic law of friction, with a static friction coefficient μ_s and a kinetic friction coefficient $\mu_d < \mu_s$. We place the origin of x at the center of the contact, which therefore extends between $\pm\frac{L}{2}$. The problem is made dimensionless by expressing coordinates in units of L, forces in units of $\mu_s N$ and stresses in units of $\frac{\mu_s N}{wL}$. Dimensionless quantities bear a tilde. We find that all physical quantities can be expressed in terms of only two dimensionless control parameters: $r = \frac{\mu_d}{\mu_s}$ and $g = 6\mu_d\frac{H}{L}$.

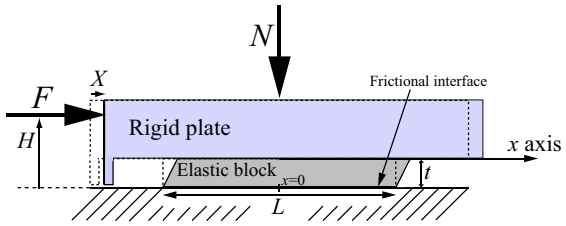

FIG. 1: Sketch of the system geometry (see text for details) for $X = 0$ (dashed line) and $X \neq 0$ (solid line).

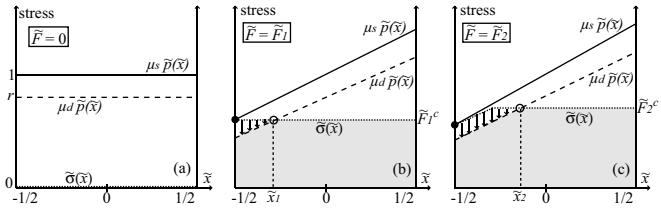

FIG. 2: Stress fields $\mu_s\tilde{p}(\tilde{x})$ (solid line), $\mu_d\tilde{p}(\tilde{x})$ (dashed line) and $\tilde{\sigma}(\tilde{x})$ (dotted line). (a) $\tilde{F}=0$: all fields are homogeneous and $\tilde{\sigma}(\tilde{x})=0$. (b) $\tilde{F}=\tilde{F}_1$: $\mu_s\tilde{p}=\tilde{\sigma}=\tilde{F}_1^c$ at $\tilde{x}=-1/2$ (black disk). Propagation stops at x_1 (open disk) where $\mu_d\tilde{p}=\tilde{\sigma}=\tilde{F}_1^c$. Vertical arrows show the stress relaxation on the segment $[-1/2;\tilde{x}_1]$. The grey surface represents the relaxed force $\tilde{F}_1^*$. (c) Same as (b) but for $\tilde{F}=\tilde{F}_2$.

We neglect any edge effect like *e.g.* a divergence of the stresses at the border of the punch-like contact [13], an assumption that is increasingly valid as t/L decreases. These edge effects would be symmetric with respect to $\tilde{x}=0$ and hence could not account alone for the observed asymmetry. Under these conditions, for $\tilde{F}=0$ the pressure field $\tilde{p}(\tilde{x})=\frac{1}{\mu_s}$ is therefore constant (Fig. 2(a)). Moreover, between two micro-slip events, the tangential displacement of the top surface of the layer is homogeneous, so that the shear stress field $\tilde{\sigma}(\tilde{x})$ increases homogeneously (Fig. 2(b)).

For $\tilde{F}\neq 0$, a torque FH is applied at the interface, which can only be balanced by an asymmetry of the pressure field. The rigid plate undergoes a slight tilt, which yields a linear spatial distribution of the pressure $\tilde{p}(\tilde{x},\tilde{F})=\frac{1}{\mu_s}+\frac{2g}{\mu_d}\tilde{F}\tilde{x}$ [24]. We assume that this form remains true even after microslips, *i.e.* the pressure field, just like the torque, depends only on the total friction force $\tilde{F}$ and not on the spatial distribution of shear stress over the contact. This assumption is similar to the classical Goodman assumption in contact mechanics [13, 18] and is here increasingly valid with decreasing t/L.

At a certain force $\tilde{F}=\tilde{F}_1$ the local static slip threshold $\tilde{\sigma}(\tilde{x})=\mu_s\tilde{p}(\tilde{x},\tilde{F})$ is reached for the first time at the trailing edge $\tilde{x}=-\frac{1}{2}$ (if $g>0$), where the pressure is minimum (black disk in Fig. 2(b)), and we find that:

$$\tilde{F}_1=\frac{1}{1+g/r}. \tag{1}$$

A micro-slip front nucleates at the trailing edge and propagate towards the leading edge through all $\tilde{x}$ such that $\tilde{\sigma}(\tilde{x})\in[\mu_d\tilde{p};\mu_s\tilde{p}]$, which are metastable. We assume that the friction force relaxation associated with the micro-slip occurs only after propagation is over. The front therefore arrests at point $\tilde{x}_1$ such that $\tilde{\sigma}(\tilde{x}_1)=\mu_d\tilde{p}(\tilde{x}_1,\tilde{F}_1)$ (open disk in Fig. 2(b)).

In all the slipped region, the shear stress drops to $\mu_d\tilde{p}(\tilde{x},\tilde{F}_1)$ (arrows in Fig. 2(b)) so that the shear stress field is now $\tilde{\sigma}(\tilde{x})=r+2g\tilde{F}_1\tilde{x}$ for $\tilde{x}\in[-1/2;\tilde{x}_1]$ and $\tilde{\sigma}(\tilde{x})=\tilde{F}_1$ elsewhere [25]. The relaxed friction force $\tilde{F}_1^*$ is the integral of this relaxed shear stress field (grey area in Fig. 2(b)). The subsequent evolution for increasing $\tilde{F}$ is a series of micro-slip events following the same scenario (see Fig. 2(c) for a sketch of the second event).

We now derive the iteration formulae for the successive values of $\tilde{F}_i$ for such precursors, the corresponding arrest positions $\tilde{x}_i$ and the relaxed forces $\tilde{F}_i^*$. We introduce the elastic force $F^c=KX$, where K is the effective stiffness of the elastic block. F^c is the tangential force that would have been required to move the rigid plate in the absence of partial relaxations related to the micro-slip events. Before macroscopic motion, $\tilde{F}^c$ reduces to $\tilde{\sigma}(\tilde{x}=1/2)$ (see Fig. 2). The value $\tilde{F}_i^c$ at the onset of the i^{th} precursor is:

$$\tilde{F}_i^c=\tilde{F}_i+\sum_{j=1}^{i-1}\left(\tilde{F}_j-\tilde{F}_j^*\right)\qquad(\tilde{F}_1^c=\tilde{F}_1). \tag{2}$$

The arrest point for the i^{th} event is then given by $\mu_d\tilde{p}(\tilde{x}_i,\tilde{F}_i)=\tilde{F}_i^c$ (see Fig. 2 (b) and (c)), yielding:

$$\tilde{x}_i=\left(\tilde{F}_i^c-r\right)/2g\tilde{F}_i. \tag{3}$$

Knowing $\tilde{F}_i$, $\tilde{F}_i^c$ and $\tilde{x}_i$, the relaxed force $\tilde{F}_i^*$ is derived by integrating the shear stress field just after the precursor. It can be easily shown graphically (see grey areas in Fig. 2(b) and (c)) that:

$$\tilde{F}_i^*=\tilde{F}_i^c-\frac{1}{2}\left(\tilde{x}_i+1/2\right)\left[\tilde{F}_i^c-r+g\tilde{F}_i\right] \tag{4}$$

The last step is to calculate the force at the next event. The first point to reach the static threshold is always at $\tilde{x}=-\frac{1}{2}$. $\tilde{F}_{i+1}$ is then such that $\mu_d\tilde{p}(-\frac{1}{2},\tilde{F}_i)+\tilde{F}_{i+1}-\tilde{F}_i^*=\mu_s\tilde{p}(-\frac{1}{2},\tilde{F}_{i+1})$, which yields:

$$\tilde{F}_{i+1}=\frac{1-r+\tilde{F}_i^*+g\tilde{F}_i}{1+g/r}. \tag{5}$$

The evolution of the system can be solved iteratively with Eq. 1 as the starting point. At each step, $\tilde{F}_i^*$, $\tilde{F}_{i+1}$, $\tilde{F}_{i+1}^c$ and $\tilde{x}_{i+1}$ are computed successively. This procedure has to be slightly modified as soon as $\tilde{x}_{n+1}>1/2$, i.e. when the $(n+1)^{th}$ event first reaches the leading edge after n precursors. At this point, the shear stress relaxes to $\tilde{\sigma}(\tilde{x})=\mu_d\tilde{p}(\tilde{x})$ everywhere, *i.e.* $\tilde{F}_{n+1}^*=r$. The subsequent evolution is then obtained by simply replacing Eq. 3 by $\tilde{x}_i=1/2$ and Eq. 4 by $\tilde{F}_i^*=r$ in the iteration.

Results - Figure 3 shows how the friction force $\tilde{F}$ typically evolves with the elastic force $\tilde{F}^c$ (which is proportional to the prescribed displacement X). This loading curve exhibits an initial elastic regime at low forces. It is followed by a series of n relaxations corresponding to n precursors of increasing length. The system then enters a macroscopic stick-slip motion regime (each slip event involves the whole interface), in which the relaxed force

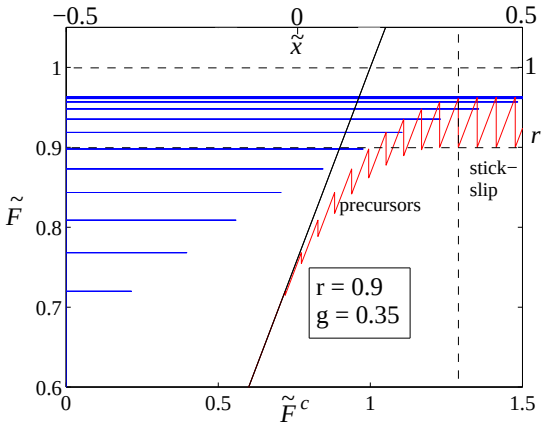

FIG. 3: Red : loading curve $\tilde{F}(\tilde{F}^c)$ ($r = 0.9$, $g = 0.35$). Black: ideal elastic loading. Blue horizontal lines: extension of the successive precursors along the contact.

is always r. Stick-slip progressively becomes periodic, reaching a maximum friction force of $\tilde{F}_{max} = \frac{1}{1+\frac{g}{r}(1-r)}$ (calculated by imposing $\tilde{F}_{i+1} = \tilde{F}_i$ in Eq. 5).

In practice, the two control parameters can only be varied over the range $0 < r < 1$ ($r > 1$ is not physical because $\mu_s > \mu_d$) and $0 < g < 1$ ($\tilde{p} > 0$ everywhere in the contact in the absence of adhesive forces, which translates into the condition that, for all $\tilde{F} < \tilde{F}_{max}$, $\tilde{p}(-1/2, \tilde{F}) > 0$, yielding $r - g\tilde{F}_{max} > 0$ and eventually $g < 1$). Figure 4 shows the number of precursors n over the whole accessible parameter space. n increases with both r and g. In particular, the larger the torque, the more precursors. Below the line $g = (1 - r)/2$, the extension of the first precursor $\tilde{x}_1$ is longer than the contact size, so that no precursor is observed. In particular, no precursor can occur at a torque-free interface ($H = 0$, i.e. $g = 0$).

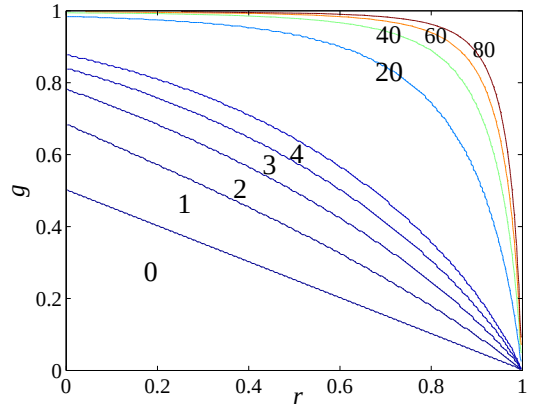

FIG. 4: Number of precursors as a function of r and g.

Discussion - We have presented a *minimal* model that accounts for the rich kinematics of the transition from static to kinetic friction. The strongest assumption made is that the motion of the micro-slip front is so fast that the associated force relaxation occurs only after its arrest. This is a hidden assumption about the propagation dynamics, which is otherwise explicitly beyond the scope of this quasistatic model [26]. In this respect, our model is a crude description of a real frictional interface. However, we believe that it captures important generic aspects of sheared frictional interfaces.

An important component of the present model is the build up of a friction-induced torque. We emphasize that in typical situations, a significant torque corresponds only to a very slight tilt angle [27]. The asymmetry of the contact is therefore very difficult to avoid experimentally.

Even for an initially homogeneous interface, tangential loading produces an increasing pressure asymmetry at the interface. In practice, the friction force is usually applied above the interface ($H > 0$), making the pressure lower at the trailing edge. Under these conditions, any friction law that prescribes a monotonic increase in shear strength with increasing local pressure implies that the lowest shear strength is at the trailing edge. In practice most friction laws belong to this category. Here, we considered the classical Amontons' law of friction, which is known to be valid for macroscopic multicontact interfaces [1, 19] [28]. Our results are therefore directly relevant to the kind of interface studied by Rubinstein *et al* [15, 17]. The smooth glass-on-gel interfaces used by Baumberger *et al* [14], although a very different system, also obey a pressure-increasing shear strength law, which is a modified version of Amontons' law including adhesive forces. Our model successfully explains why micro-slip fronts always occur at the trailing edge in both systems.

Rubinstein *et al* provide data for the distribution of area of real contact just after the successive precursors and after each slip in the periodic stick-slip regime (Fig. 4(a) in [15]). In a multicontact interface, the real area of contact is well-known to be proportional to the applied contact pressure [19, 20]. Our model provides a simple explanation for their observation of a pressure asymmetry which increases with F, and which is retained and stable in the macroscopic stick-slip regime, with a minimum pressure near the trailing edge.

Quantitative comparison between our model and Rubinstein *et al*'s measurements for the number and length of the precursors is not possible because the two loading systems are very different. They push directly on the side of a slider, making the shear stress much higher near the trailing edge than elsewhere, as modeled in [9]. However, we believe that the kinematics of their transition from statics to stick-slip, including precursors could be understood using the principles employed in the present model and comparing locally the pressure and shear fields. These fields would correspond to the Hertz-

like stress field around the loaded point. Even in the same geometry, quantitative comparison requires knowledge of the effective height H of the applied friction force, which is seldom provided in the literature (see *e.g.* [21] for an exception, where H is set to 0).

An implication of the fact that micro-slip very generically nucleates at the trailing edge of a contact implies that the interface will be in a compressed state as soon as the first precursor occurs. This strongly suggests that the results of Bennewitz *et al* [16], which measure such compression, are valid over a much broader range of systems than their microstructured PDMS on glass interface.

Other results of the model are of general interest for frictional systems. First, they suggest that, from a kinematic point of view, macroscopic stick-slip is not different from the preceding precursors, the latter being merely defined by their limited extent over the interface. Second, we show that F_{max}/N is always smaller than μ_s, *i.e.* the macroscopic friction coefficient is always lower than the local friction coefficient, which governs the onset of the micro-slip instability. The macroscopic friction coefficient is moreover dependent on g, *i.e.* on the details of the loading system, suggesting that care has to be taken when a friction coefficient is measured using a macroscopic experiment.

We have shown that in virtually all friction experiments, slip will occur at an asymmetrically loaded interface due to a friction-induced torque. In particular, the pressure is minimum near the trailing edge, where all micro-slip instabilities nucleate. The *kinematics* of the transition from static to stick-slip friction is then dominated by this macroscopic, system-dependent, asymmetry rather than by small scale heterogeneities of the shear strength. This is in striking contrast with most friction models, which assume a homogeneously loaded interface bearing a relatively small disorder (see *e.g.* [7, 9]). In this respect, the present work provides a framework for the extension of these models to take into account a macroscopic shear strength asymmetry.

We acknowledge funding from the European Union through grant PIEF-GA-2009-237089. We thank E. Barthel, G. Debrgeas, A. Malthe-Sørenssen, P. Meakin and F. Renard for discussions.

* Electronic address: julien.scheibert@fys.uio.no

[1] B. Persson, *Sliding Friction* (Springer, 2000).
[2] M. Urbakh, J. Klafter, D. Gourdon, and J. Israelachvili, Nature **430**, 525 (2004).
[3] T. Baumberger and C. Caroli, Adv. Phys. **55**, 279 (2006).
[4] B. Bhushan, *Nanotribology and Nanomechanics* (Springer, Heidelberg, Germany, 2008).
[5] C. Scholz, *The Mechanics of Earthquakes and Faulting* (Cambridge University Press, 2002).
[6] J. Scheibert, S. Leurent, A. Prevost, and G. Debrégeas, Science **323**, 1503 (2009).
[7] R. Burridge and L. Knopoff, Bull. Seismol. Soc. Am. **57**, 341 (1967); J. M. Carlson and J. S. Langer, Phys. Rev. Lett. **62**, 2632 (1989); Z. Olami, H. J. S. Feder, and K. Christensen, Phys. Rev. Lett. **68**, 1244 (1992).
[8] H. Kanamori and E. E. Brodsky, Rep. Prog. Phys. **67**, 1429 (2004); E. A. Brener, S. V. Malinin, and V. I. Marchenko, Eur. Phys. J. E **17**, 101 (2005); F. Brochard-Wyart and P. de Gennes, Eur. Phys. J. E **23**, 439 (2007).
[9] O. Braun, I. Barel, and M. Urbakh, Phys. Rev. Lett. **103**, 194301 (2009).
[10] A. J. Rosakis, O. Samudrala, and D. Coker, Science **284**, 1337 (1999).
[11] S. M. Rubinstein, G. Cohen, and J. Fineberg, Nature **430**, 1005 (2004).
[12] J. Scheibert, G. Debrégeas, and A. Prevost, Arxiv:0809.3188v1 (2008); A. Chateauminois, C. Fretigny, and L. Olanier, Phys. Rev. E **81**, 026106 (2010).
[13] K. L. Johnson, *Contact Mechanics* (Cambridge University Press, 1985).
[14] T. Baumberger, C. Caroli, and O. Ronsin, Phys. Rev. Lett. **88**, 075509 (2002); T. Baumberger, C. Caroli, and O. Ronsin, Eur. Phys. J. E **11**, 85 (2003).
[15] S. M. Rubinstein, G. Cohen, and J. Fineberg, Phys. Rev. Lett. **98**, 226103 (2007).
[16] R. Bennewitz, J. David, C. F. de Lannoy, B. Drevniok, P. Hubbard-Davis, T. Miura, and O. Trichtchenko, J. Phys.: Condens. Matter **20**, 015004 (2008).
[17] S. M. Rubinstein, G. Cohen, and J. Fineberg, J. Phys. D: Appl. Phys. **42**, 214016 (2009).
[18] J. Scheibert, A. Prevost, G. Debregeas, E. Katzav, and M. Adda-Bedia, J. Mech. Phys. Solids **57**, 1921 (2009).
[19] B. N. J. Persson, I. M. Sivebaek, V. N. Samoilov, K. Zhao, A. I. Volokitin, and Z. Zhang, J. Phys.: Condens. Matter **20**, 395006 (2008).
[20] J. A. Greenwood and J. B. P. Williamson, Proc. R. Soc. Lond. A **295**, 300 (1966).
[21] L. Bureau, T. Baumberger, and C. Caroli, Phys. Rev. E **62**, 6810 (2000).
[22] J. Scheibert, et al., to be published.
[23] J. Scheibert, A. Prevost, J. Frelat, P. Rey, and G. Debrégeas, Europhys. Lett. **83**, 34003 (2008).
[24] Linearity was checked using finite element calculations.
[25] The slope discontinuity of the shear stress at $\tilde{x}_1$ is regularized over a length $\sim t$.
[26] We simulated the opposite situation of a slow micro-slip front such that F and the pressure gradient are relaxed at each increment of length [22]. Comparison between the fast and slow micro-slip models shows the robustness of all the qualitative results of the present work: nucleation at the trailing edge, pressure asymmetry and precursors prior to macroscopic stick-slip motion. Of course, the values of $\tilde{F}_i$ and $\tilde{x}_i$ obtained from the two models differ, and this alters the boundaries between regions in Fig. 4.
[27] *e.g.* for small deformations $F/wLE < 10^{-3}$, a force applied at the bottom of the rigid plate $H = h$ and an aspect ratio $h/L < 10^{-1}$, $\alpha < 1.2 \cdot 10^{-4}$rad.
[28] We therefore neglect any effect of the tangential stiffness of the multicontact interface, which induces deviations to Amontons in contacts where stick and slip regions coexist [23]. We also neglect state and rate dependencies of the friction coefficients [3].